Density functional calculations of the electronic structure and optical properties of the ternary carbides Al_4SiC_4 and $Al_4Si_2C_5$

Altaf Hussain,[1,*] Sitaram Aryal,[2] Paul Rulis,[2] M. Arshad Choudhry,[1] and W. Y. Ching[2]
[1]*Department of Physics, The Islamia University of Bahawalpur, Punjab, Pakistan*
[2]*Department of Physics, University of Missouri-Kansas City, Missouri 64110, USA*
(Received 22 July 2008; published 5 November 2008)

The electronic structure and spectroscopic properties of two ternary aluminum silicon carbide ceramics Al_4SiC_4 and $Al_4Si_2C_5$ are studied by density functional theory calculations based on the orthogonalized linear combination of atomic orbitals method. Both crystals are shown to be small gap semiconductors with indirect band gaps of 1.05 and 1.02 eV, respectively. The calculated hole and electron effective mass and the interband optical properties, in the form of the complex dielectric function, show a high degree of anisotropy which can be traced to the unique structures of these two crystals. The calculated refractive indices are consistent with the values proposed in the literature. Mulliken effective charge and bond order calculations show that these crystals have a high degree of covalency with considerable charge transfer from Al and Si to the C atoms. The x-ray absorption near-edge-structure for all crystallographically nonequivalent sites (*K* and *L* edges) is calculated and compared with those of cubic SiC. It is shown that the site-averaged Si-*K* and Si-L_3 edges, and also the C-*K* edges are slightly different and broader than those of cubic SiC. Potential applications of these ternary ceramics are also discussed.

DOI: 10.1103/PhysRevB.78.195102 PACS number(s): 71.20.Ps, 78.40.Ha

I. INTRODUCTION

A large number of aluminum-containing ternary ceramics are among the most promising candidates for high-temperature structural applications, especially in oxidation-protective multicomposition coatings.[1] Layered ternary aluminum carbides (e.g., Ti_3AlC_2, Ti_2AlC, and Nb_2AlC) have been reported to be hexagonal crystals with many desirable properties such as room-temperature ductility, oxidation resistance, and high damage tolerance, in favorable comparison to their binary counterparts.[2] Another group of hexagonal ternary aluminum carbides in the Zr-Al-C and Hf-Al-C systems has also been studied in 1980s.[3] By means of first-principles pseudopotential total-energy calculations, the mechanical properties and electronic structure of $Zr_3Al_3C_5$ was recently studied by Wang *et al.*[4] The calculated equation of state, elastic parameters, ideal tensile, and shear strengths were reported to be similar to the hard binary carbide, ZrC.

Another important class of ternary ceramic carbides is the Al-Si-C system. Because of their superior properties such as good wear resistance, high strength, and high thermal conductivity; the Al-Si-C-based ceramic materials have been widely used not only in weight sensitive applications but also as heat-exchange materials in modern power electronics.[5,6] Among them, Al_4SiC_4 has the most outstanding properties including a high melting point (~ 2080 °C), low density (3.03 g/cm^3), and excellent oxidation and corrosion resistance.[7,8] Its oxidation behavior, electrical conductivities, and mechanical properties, particularly the enhanced fracture toughness at room temperature and the increased bending strength at high temperatures in air have been studied extensively.[9–14] It has been recognized as an important compound in the technology of aluminum composite materials.[15] Very recently, Liao *et al.*[16] studied the atomistic deformation modes and elastic properties of Al_4SiC_4 using the first-principles pseudopotential method. Based on their calculated data, it was concluded that the structural failure occurring in tensile deformation simulation is due the existence of intrinsic brittleness in this crystal, which in term is related to its electronic structure and bonding. In 1980, Inoue *et al.*[17] synthesized a new phase of aluminum silicon carbide, $Al_4Si_2C_5$, by mixing silicon carbide and Al_4C_3 with a ball mill made of polyethylene, and reported the full crystal structure of this new compound. So far, no other experimental or theoretical studies on $Al_4Si_2C_5$ have been reported for this relatively new phase. To our knowledge, no theoretical investigations of the electronic structures and optical properties of these two important ternary carbides have been reported. In this paper, we report the *ab initio* calculations of the electronic structure, bonding, and spectroscopic properties of Al_4SiC_4 and $Al_4Si_2C_5$ crystals using the first-principles orthogonalized linear combination of atomic orbitals method (OLCAO).[18]

The paper is organized as follows: in Sec. II, we discuss the crystal structures of Al_4SiC_4 and $Al_4Si_2C_5$. We briefly outline our method of calculations in Sec. III. In Sec. IV, we present and discuss the calculated results. The paper ends with a summary of the results obtained and presents our conclusions.

II. CRYSTAL STRUCTURE

Al_4SiC_4 and $Al_4Si_2C_5$ are both hexagonal crystals with space groups $P6_3mc$ (No. 186) and $R3m$ (No. 160), respectively.[17,19,20] The unit cell of Al_4SiC_4 has 2 f.u. with a total of 18 atoms, whereas $Al_4Si_2C_5$ has 3 f.u. in the unit cell with 33 atoms. The crystal structure of $Al_4SiC_4/Al_4Si_2C_5$ is isostructural with $Al_5C_3N/Al_6C_3N_2$ and consists of Al_4C_3 and SiC layers. The SiC layers are similar to AlN layers in the Al_5C_3N.[19,20] The crystal structures of Al_4SiC_4 and $Al_4Si_2C_5$ are depicted in Fig. 1. Al_4SiC_4 has nine nonequivalent atomic sites (four Al, one Si, and four C), while

 ©2008 The American Physical Society

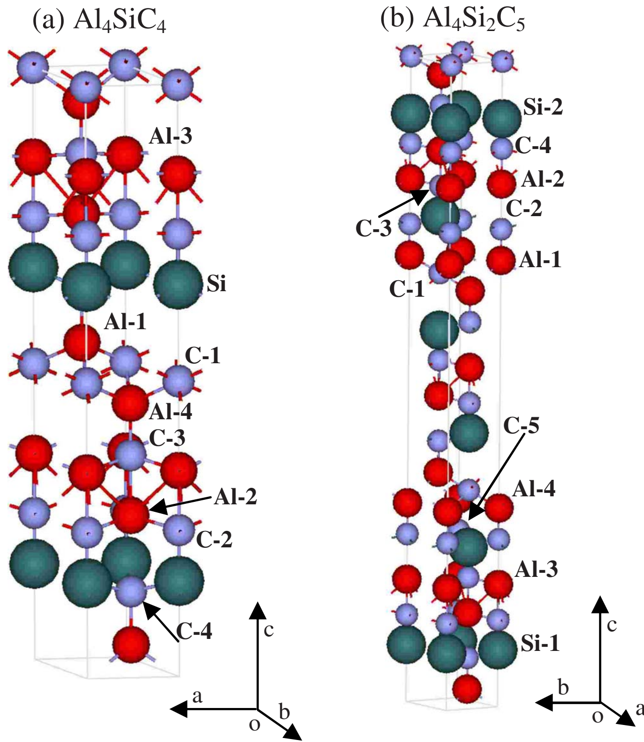

FIG. 1. (Color online) Crystal structures of (a) Al_4SiC_4, and (b) $Al_4Si_2C_5$. The red, dark green, and blue balls represent Al, Si, and C atoms, respectively.

$Al_4Si_2C_5$ has eleven nonequivalent atomic sites (four Al, two Si, and five C).

The lattice constants and atomic positions of these ternary carbides used in our calculations were taken from Inoue *et al.*[19] These structures were then optimized using the Vienna *ab initio* Simulation Package (VASP).[21] VASP is a simulation package based on density functional theory (DFT). It is an efficient and reliable tool for the atomic relaxation and geometry optimization. In the present study, the optimization was carried out with accurate precision and an adequate energy cutoff of 500 eV. The Davidson block iteration scheme[22] was used for the optimization of the wave function, and the ultrasoft pseudopotential with generalized gradient approximation (GGA) for the exchange-correlation potential was adopted.[23,24] For k-space sampling we have used a $4 \times 4 \times 1$ Monkhorst-pack[25] mesh. A relatively high accuracy for the ground-state electronic convergence (10^{-5} eV) and a small tolerance for the ionic relaxation convergence (10^{-3} eV) were used.

The crystal structure parameters for these two crystals are summarized in Table I. It can be seen that the VASP relaxed structures are very close to the experimentally determined parameters, differing by no more than 0.55%. The local environments near the Al-2 atoms and the Si atoms in the two crystals are shown in Fig. 2. As can be seen, the bond lengths (BLs) and the bond angles (BAs) of the local tetrahedral units are highly distorted. The local atomic geometry in these two crystals will be discussed later in connection with bond order calculations.

TABLE I. Structure parameters and atom types of ternary carbides Al_4SiC_4 and $Al_4Si_2C_5$.

	Al_4SiC_4	$Al_4Si_2C_5$
Crystal type	Hexagonal	Hexagonal
Space group	$P6_3mc$(No.186)	$R3m$(No.160)
Lattice parameters		
a(Å)	3.277[a](3.282[b])	3.251[a](3.244[b])
b(Å)	3.277[a](3.282[b])	3.251[a](3.244[b])
c(Å)	21.676[a](21.796[b])	40.108[a](40.310[b])
α	90.00[a](90.00[b])	90.00[a](90.00[b])
β	90.00[a](90.00[b])	90.00[a](90.00[b])
γ	120.00[a](119.99[b])	120.00[a](119.99[b])

[a]Reference 19.
[b]Data obtained after VASP relaxation.

III. METHOD OF CALCULATIONS

The VASP relaxed crystal structures were used to calculate the electronic structures and optical properties of the two ternary carbides using the OLCAO method. OLCAO is a density-functional-theory–based method that uses the local-density approximation (LDA) for the exchange-correlation potential. The method is particularly effective for materials with complex structures[26–29] and has been extensively used in the study of a variety of crystalline and noncrystalline materials. The method has been well described in many published papers [e.g., Ref. 18] and will not be repeated here. In the present calculations, we used the full basis set which

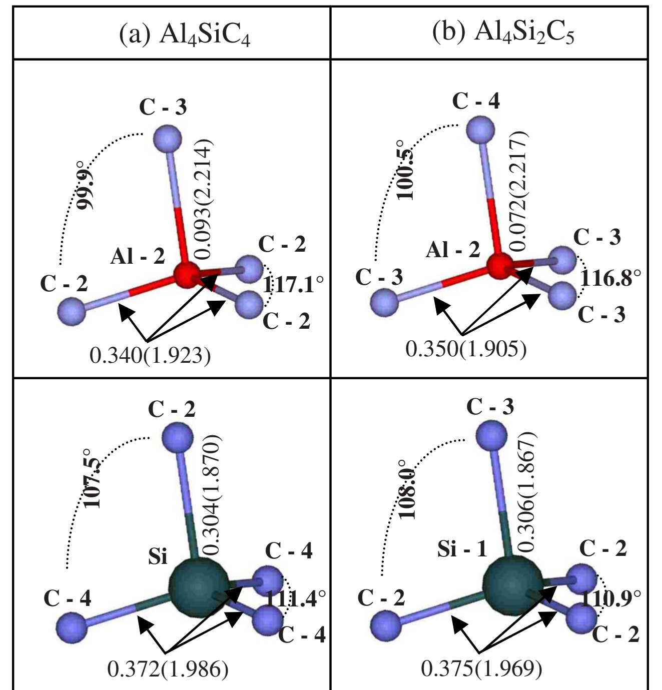

FIG. 2. (Color online) Bonding features of (a) Al_4SiC_4, and (b) $Al_4Si_2C_5$. The values in parenthesis are the bond lengths (in angstrom), while the values outside the parenthesis are the bond order (in electron). The bond angles are also indicated.

consists of the following atomic orbitals: (1) Al, core orbitals ($1s$, $2s$, $2p$), occupied valence orbitals ($3s$, $3p$), additional empty orbitals ($4s$, $4p$, $3d$); (2) Si, core orbitals ($1s$, $2s$, $2p$), occupied valence orbitals ($3s$, $3p$), additional empty orbitals ($4s$, $4p$, $3d$); and (3) C, core orbital ($1s$), occupied valence orbitals ($2s$, $2p$), and additional empty orbitals ($3s$, $3p$). A full basis set provides sufficient variational freedom to the Bloch functions for high accuracy. A large k-point sampling (512 k points) in the irreducible portion of the Brillouin zone (BZ) was used for each crystal. The crystal potential was iterated to self-consistency when the total energy converged to within 0.0001 eV in less than 20 iterations.

One of the advantages of using the OLCAO method is the ease with which the effective charge on each atom and the bond order (BO) between each pair of atoms can be calculated based on Mulliken's scheme for population analysis.[30] The Mulliken effective charge (Q^*_α) is defined as the occupied valence electrons associated with an atom α in the crystal.

$$Q^*_\alpha = \sum_i \sum_{n,occ} \sum_{j,\beta} C^{*n}_{i\alpha} C^n_{j\beta} S_{i\alpha,j\beta}, \qquad (1)$$

where $C^n_{j\beta}$ are the eigenvector coefficients, $S_{i\alpha,j\beta}$ is the overlap integrals, n is the band index, i and j are the atomic orbitals, and α and β are the atom labels. The effective charge defined in Eq. (1) is the total number of valence electrons on the ion. Q^*_α provides information about the charge transfer (gain or loss of electronic charge from the neutral atom) and is very useful in providing physical insight for the interpretation of experimental data.

The BO between a pair of atoms α and β is defined as

$$\rho_{\alpha\beta} = \sum_{n,occ} \sum_{i,j} C^{*n}_{i\alpha} C^n_{j\beta} S_{i\alpha,j\beta}. \qquad (2)$$

The BO is a useful quantitative parameter to describe the strength of a bond between two atoms. For a covalently bonded homopolar crystal, such as Si or diamond, the BO is 0.5 (or 1 if both spins are counted) because there is no charge transfer in these crystals. For a highly ionic crystal, the BO value can be small. A negative BO value indicates antibonding states, which usually occur with next-nearest neighbor (NNN) atomic pairs. Because the Mulliken scheme is most effective when the atomic basis functions are localized, the effective charge and BO calculations were carried out separately using a minimal basis set (without extra orbitals) instead of the full basis set.

The calculation of the optical properties entails the evaluation of the imaginary component of the dielectric function according to

$$\varepsilon_2(\omega) = \left(\frac{e^2}{\pi m E \omega}\right) \times \int d\vec{k} \sum_{n,l} |\langle \psi_n(\vec{k},\vec{r}) | \vec{P} | \psi_l(\vec{k},\vec{r}) \rangle|^2 f_l(\vec{k}) \times [1 - f_n(\vec{k})] \delta[E_n(\vec{k}) - E_l(\vec{k}) - E], \qquad (3)$$

where $E=\hbar\omega$ is the photon energy, $f(\vec{k})$ is the Fermi distribution function, and l labels an occupied state and n an unoccupied state. The square of the momentum matrix element (MME) $\langle \psi_n(\vec{k},\vec{r}) | \vec{P} | \psi_l(\vec{k},\vec{r}) \rangle$ in Eq. (3) has three Cartesian components. The anisotropy of the imaginary component of the dielectric function can be studied by resolving the square of the MME in a specific Cartesian direction. The real part of the dielectric function can be obtained from the imaginary part by Kramers-Kronig conversion.

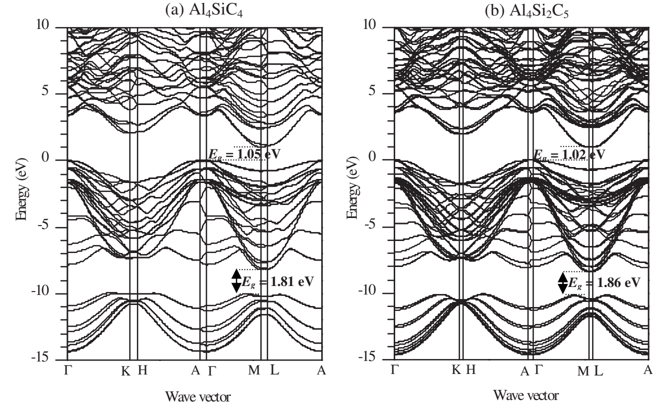

FIG. 3. Band structures of (a) Al_4SiC_4, and (b) $Al_4Si_2C_5$. Energy of the top of the valence band is set at zero.

IV. RESULTS AND DISCUSSION

A. Electronic structure and bonding

The calculated band structures of Al_4SiC_4 and $Al_4Si_2C_5$ crystals are shown in Fig. 3. The two band structures are very similar with a slight difference in the indirect band gap (E_g) value, which is smaller in $Al_4Si_2C_5$ than in Al_4SiC_4. The top of the valence band (VB) is at the Γ point, while the bottom of the conduction band (CB) is at M point in both crystals giving the indirect-gap value of 1.05 and 1.02 eV, respectively, for Al_4SiC_4 and $Al_4Si_2C_5$. These gap values are expected to be smaller than the real gap values since it is well known that LDA calculations generally underestimate the band gaps.[31] The effective mass of the electron and hole along the parallel ($m^*_\parallel$) and the perpendicular ($m^*_\perp$) directions to the c axis are calculated from the band curvatures at M and Γ points. They are listed in Table II. The calculated electron effective-mass ratios (m^*/m_e) for Al_4SiC_4 and $Al_4Si_2C_5$ are 0.620 and 0.619 (0.554 and 3.060) perpendicular (parallel) to the c axis. They are smaller than Si (1.08), comparable to that of Ge (0.55), and larger than GaAs (0.067) and InSb (0.013). On the other hand the calculated hole effective-mass values in Al_4SiC_4 and $Al_4Si_2C_5$ are 2.984 and 3.100 (14.540 and 30.770) perpendicular (parallel) to the c axis. These values are much larger than Si (0.56), Ge (0.37), GaAs (0.45), and InSb (0.6) crystals.[32,33] The large hole effective masses are consistent with the flat band structure at the top of the VB. It should be pointed out that the effective masses calculated from the band curvatures along different symmetry directions are not affected by the gap under estimation due to the deficiency in the LDA-DFT. The difference in $m^*_\perp$ and $m^*_\parallel$ values confirms the anisotropic behavior of the two crystals. From the calculated values, it is noted that the parallel component of the electron effective mass in $Al_4Si_2C_5$ is much larger than in Al_4SiC_4. This could

TABLE II. Effective charge (Q^*), and refractive index data for Al_4SiC_4 and $Al_4Si_2C_5$.

Al_4SiC_4		$Al_4Si_2C_5$	
Effective charge (electrons)			
Al		Al	
Min Q^*	2.000	Min Q^*	1.993
Max Q^*	2.182	Max Q^*	2.145
Mean Q^*	2.098	Mean Q^*	2.070
Charge transfer (ΔQ^*)	−0.902	Charge transfer (ΔQ^*)	−0.930
Si		Si	
Min Q^*	3.156	Min Q^*	3.146
Max Q^*	3.165	Max Q^*	3.154
Mean Q^*	3.160	Mean Q^*	3.150
Charge transfer (ΔQ^*)	−0.840	Charge transfer (ΔQ^*)	−0.850
C		C	
Min Q^*	4.937	Min Q^*	4.944
Max Q^*	5.184	Max Q^*	5.189
Mean Q^*	5.111	Mean Q^*	5.084
Charge transfer (ΔQ^*)	+1.111	Charge transfer (ΔQ^*)	+1.084
Band gap (eV)	1.05		1.02
Energy gap between lower and upper parts of VB (eV)			
VB width (eV)	1.81		1.86
Upper part	7.090		8.076
Lower part	3.272		3.564
$\varepsilon_1(0)$			
Parallel	6.134		6.108
Perpendicular	16.149		16.380
Refractive index (n)	2.73 (2.5^a)		2.74
Effective mass (m_e)			
$m_\perp^*(electron)$	0.620		0.619
$m_\parallel^*(electron)$	0.554		3.060
$m_\perp^*(hole)$	2.984		3.100
$m_\parallel^*(hole)$	14.540		30.770

[a] Reference 36.

be related to the much larger c-axis dimension in $Al_4Si_2C_5$ and somewhat different stacking sequences in the c direction. This seems to imply that the movements of the electrons in $Al_4Si_2C_5$ are effectively limited to the perpendicular direction only.

The calculated total density of states (TDOS) and atom-resolved partial density of states (PDOS) for Al_4SiC_4 and $Al_4Si_2C_5$ are shown in Figs. 4(a) and 4(b), respectively. Both spectra have many structures as a result of the complexity of the crystal structure and the presence of many nonequivalent sites. The general shapes of the TDOS in both crystals are very similar, both in the VB region and in the CB region, indicating that the fundamental bonding pictures in the two crystals are the same. The TDOS are resolved into partial DOS for atoms at the crystallographically nonequivalent sites. Although both Si and C are group IV elements, their PDOS are not the same especially in the upper region of the VB. This is related to the charge transfer from Si to C and will be further discussed below. For Al_4SiC_4, there are nine nonequivalent sites consisting of Al-1 to Al-4, Si, and C-1 to C-4, while for $Al_4Si_2C_5$ there are 11 nonequivalent sites consisting of Al-1 to Al-4, Si-1 and Si-2, and C-1 to C-5. A deeper inspection of the PDOS in each crystal system reveals that they are not identical. These differences reflect the longer range structural differences caused by different stacking sequences. The VB structure of Al_4SiC_4 and $Al_4Si_2C_5$ can be further divided into two parts separated by a gap of slightly over 1.7 and 1.6 eV, respectively. The lower part comes from the bonding between the Al 3s, Si 3s, and C 2s orbitals, while the upper one is dominated by 3p (for Al and Si) and 2p (for C) orbitals, respectively, in the familiar sp^3 hybridization of the tetrahedral bonding.

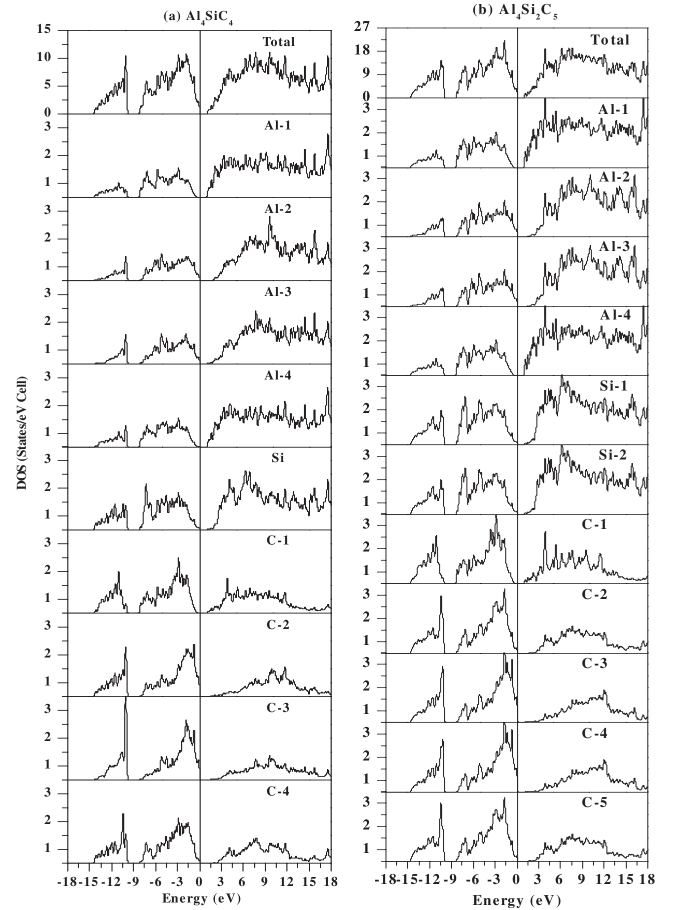

FIG. 4. Total and partial DOS plots of (a) Al_4SiC_4, and (b) $Al_4Si_2C_5$.

The calculated Mulliken effective charge, Q^*, per ion for all crystallographically nonequivalent sites in Al_4SiC_4 and $Al_4Si_2C_5$ are shown in Figs. 5(a) and 5(b), respectively. The major information about Q^* calculation is summarized in Table II. In both crystals Al and Si are losing electrons, while C gains electrons. In this sense the bonding behavior of these two systems is very similar. The amount of charge transfer from Al and Si to C is more or less the same in both crystals. In Al_4SiC_4, Al loses an average of 0.90 electrons, while Si

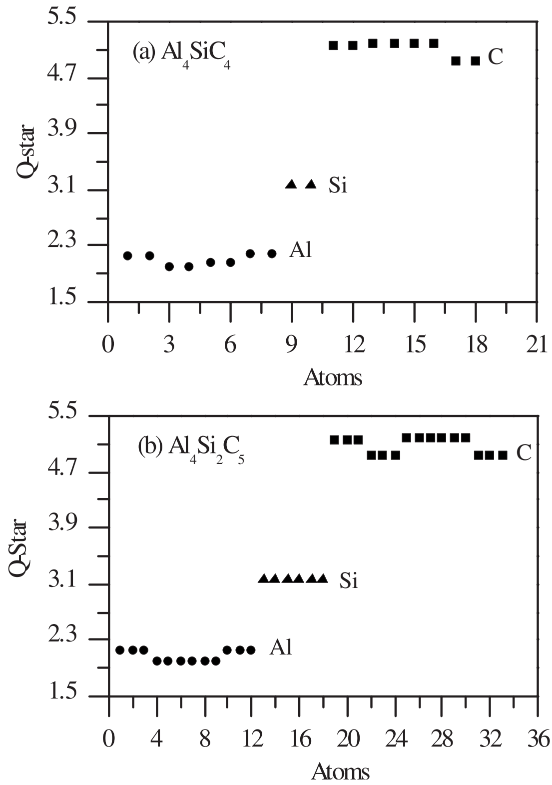

FIG. 5. Effective charge (Q^*) distribution plots of: (a) Al_4SiC_4. Atoms 1,2 belong to Al-1; 3,4 to Al-2; 5,6 to Al-3; 7,8 to Al-4; 9,10 to Si; 11,12 to C-1; 13,14 to C-2; 15,16 to C-3; and 17,18 to C-4. (b) $Al_4Si_2C_5$. Atoms 1,2,3 belong to Al-1; 4,5,6 to Al-2; 7,8,9 to Al-3; 10,11,12 to Al-4; 13,14,15 to Si-1; 16,17,18 to Si-2; 19,20,21 to C-1; 22,23,24 to C-2; 25,26,27 to C-3; 28,29,30 to C-4; and 31,32,33 to C-5 types.

loses an average of 0.84 electrons. On the other hand in $Al_4Si_2C_5$, Al and Si lose 0.93 and 0.85 electrons. The C in Al_4SiC_4 and $Al_4Si_2C_5$ gains on average 1.11 and 1.08 electrons in these two crystals, respectively. For comparison, we note that the mean Q^* values for Si and C in cubic 3C-SiC (Ref. 34) are 3.113 and 4.887 electrons, respectively, which are comparable to 3.160 and 5.111 electrons in Al_4SiC_4 and 3.150 and 5.084 electrons in $Al_4Si_2C_5$. Figure 5 also shows that Q^* for the nonequivalent atoms within each crystal are slightly different, similar to the atom-resolved PDOS shown in Fig. 4. This again indicates that the differences in structural configurations beyond the next-nearest neighbors in each crystal are fully reflected in the *ab initio* calculations. In the empirical or semiempirical types of calculations, these subtle differences are frequently ignored or cannot be accurately accounted for.

The BO values between all nearest-neighbor (NN) atomic pairs in the two crystals were calculated according to Eq. (2). Selected BO values are indicated in Fig. 2 which provides a basic bonding picture in Al_4SiC_4 and $Al_4Si_2C_5$. In Al_4SiC_4, Al-2 atoms make three short bonds (1.923 Å) with C-2 atoms and one long bond (2.214 Å) with a C-3 atom. The BO between Al-2 and C-2 is larger (0.340) than that between Al-2 and C-3 (0.093). The situation in $Al_4Si_2C_5$ is similar but with an even larger contrast in the BO values. Hence, in both crystals, the planar Al-C bonds are much stronger than the axial Al-C bonds. The situation is quite different in the Si-C_4 tetrahedra where the planar Si-C bonds (1.986 Å in Al_4SiC_4 and 1.969 Å in $Al_4Si_2C_5$) are longer than the axial Si-C bonds (1.870 Å in Al_4SiC_4 and 1.867 Å $Al_4Si_2C_5$), but the BO values show a reversed trend. The BO value for the longer bond (0.372 in Al_4SiC_4 and 0.375 $Al_4Si_2C_5$) is slightly larger than that for the shorter bonds (0.304 in Al_4SiC_4 and 0.306 in $Al_4Si_2C_5$)! These results clearly indicate that the BO value, and the strength of a bond, does not always scale with the BL. In many cases, the BA effect and to some extent, the NNN effect should also be taken into consideration. In Al_4SiC_4 the three angles C2-Al2-C2 in the planar direction are equal to 117.1°, and all vertical angles C2-Al2-C3 have the value 99.9°. This implies that the Al-2 atom is closer to the C2 plane resulting in a longer and weaker Al2-C3 bond. In the case of Si-centered tetrahedron, the C4-Si-C4 angles are 111.4° and the C2-Si-C4 angles are 107.5°, much closer to the value for a regular tetrahedron. The situation is the same in $Al_4Si_2C_5$ with only a slight difference in the bond angle values.

B. Optical properties

The optical properties of Al_4SiC_4 and $Al_4Si_2C_5$ were calculated from the band structures and the wave functions using a large k-point sampling in accordance with Eq. (3). The results are presented in the form of the frequency-dependent complex dielectric functions for photon energies up to 35 eV. The dipole matrix elements of transition are fully included. The real $[\varepsilon_1(\hbar\omega)]$ and the imaginary $[\varepsilon_2(\hbar\omega)]$ parts of the dielectric functions of the two ternary carbides are presented in Fig. 6. The spectral shapes of Al_4SiC_4 and $Al_4Si_2C_5$ are quite similar, reflecting the similarities in their electronic structures. There exists a single prominent peak in $\varepsilon_2(\hbar\omega)$ of Al_4SiC_4 at 5.82 eV. On the other hand three peaks can be identified at 5.91, 6.53, and 7.79 eV in $\varepsilon_2(\hbar\omega)$ of $Al_4Si_2C_5$. There is also a shoulder present at 4.56 eV in the $\varepsilon_2(\hbar\omega)$ of $Al_4Si_2C_5$. All these differences reflect the complex interplay of the slight differences in the electronic structure at various symmetry points of the BZ. The real part of the dielectric function shows a strong peak at 4.38 eV in Al_4SiC_4, while there are two peaks visible at 4.38 and 5.20 eV in the case of $Al_4Si_2C_5$.

For crystals with hexagonal symmetry, it is desirable to investigate the optical anisotropy by resolving $\varepsilon_2(\hbar\omega)$ into two directions, one parallel (‖) and the other perpendicular (⊥) to the c axis, or in the basal plane. These are shown in Fig. 7 revealing a large optical birefringence in both crystals. This effect can occur only if the structure of the material is highly anisotropic. The reason for birefringence is that in anisotropic media, the electric field vector $\vec{E}$, and the dielectric displacement $\vec{D}$ are not exactly parallel, although being linearly related.[35] Figure 7 shows that there is considerable optical anisotropy in the hexagonal ternary aluminum silicon carbides which could lead to potential applications in optoelectronics.

The real parts of the dielectric functions in the ternary carbides Al_4SiC_4 and $Al_4Si_2C_5$ are obtained from the imaginary parts [Eq. (3)] by Kramers-Kronig conversion. The

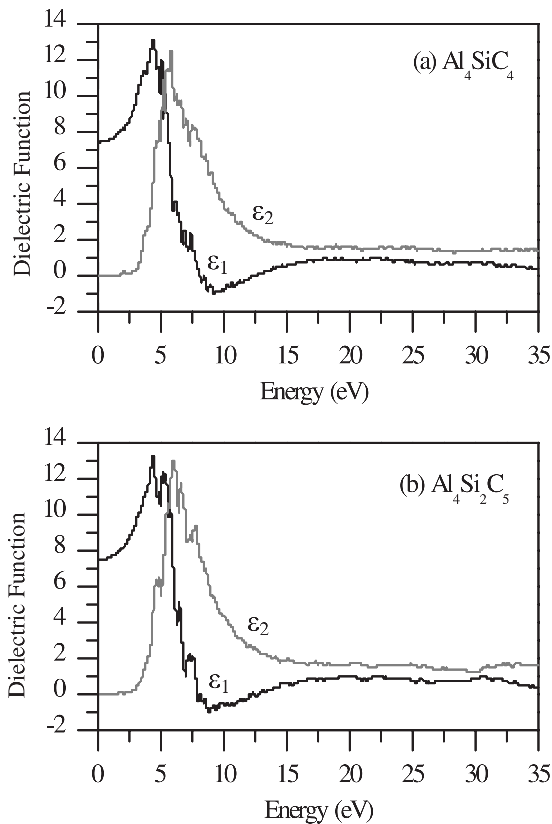

FIG. 6. Calculated real (ε_1) and imaginary (ε_2) parts of the dielectric functions of (a) Al_4SiC_4, and (b) $Al_4Si_2C_5$.

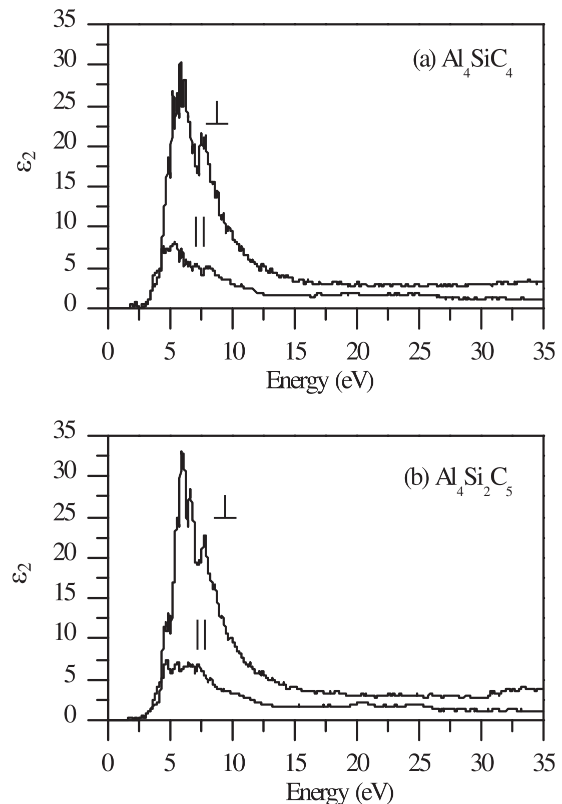

FIG. 7. Calculated parallel (∥) and perpendicular (⊥) components of the imaginary part of the dielectric function of (a) Al_4SiC_4, and (b) $Al_4Si_2C_5$.

$\varepsilon_1(\hbar\omega)$ is sensitive to the energy ranges covered for $\varepsilon_2(\hbar\omega)$. Since $\varepsilon_2(\hbar\omega)$ calculated at higher photon energies are generally less accurate due to the finite basis set used, the real part $\varepsilon_1(\hbar\omega)$ obtained from Kramers-Kronig analysis has a certain degree of uncertainty. This will be best judged by the value in the zero-frequency limit of $\varepsilon_1(\hbar\omega)$, $\varepsilon_1(0)$ which is generally referred to as the electronic part of the static dielectric constant, or the optical dielectric constant. It is related to the refractive index of the crystal by $n=\sqrt{\varepsilon_1(0)}$. The calculated values of n are listed in Table II together with the proposed values in the literature.[36] They are in reasonable agreement. $\varepsilon_1(0)$ is further decomposed into parallel and perpendicular components and are listed in Table II.

C. X-ray absorption near-edge structure or energy-loss near-edge structure spectral calculation

In recent years, x-ray absorption near-edge structure (XANES) spectroscopy has been widely used for materials characterization. Many powerful synchrotron radiations center have been built in many countries over the world for research on all kinds of materials. At the same time, electron energy-loss spectroscopy has evolved into a powerful technique to study material properties at the atomic level.[37] In particular, the energy-loss near-edge structure (ELNES) observed in the inner-shell ionization process is a powerful tool for material characterization. Although the instrumentation or the facilities used in these two techniques differ widely, the theory of inelastic scattering involved in these two experimental probes is very similar with the exception of the incoming scattering particles, i.e., photons vs electrons. Generally speaking, XANES measurements can give a higher-energy resolution than ELNES measurements, but will require large national facilities and associated instrumentation. On the other hand, the ELNES is more accessible and can be obtained by using dedicated analytical transmission electron microscopy together with high-resolution images in real space. With a realistic goal of having a subangstrom resolution, ELNES spectra can show a rich variety of structures that can be correlated with the structure and composition of the material under study. Hence, both XANES and ELNES can provide useful information about site occupancy, chemical shift of a given element, as well as information about interatomic bonding. To help interpret the experimental data, many theoretical methods have been developed to calculate the XANES or ELNES spectra. One of the methods is the supercell OLCAO method.[38] This is a very robust and accurate method which takes into account the core-hole effect and has been applied to many crystals[39–41] and systems containing defects.[42,43] Most recently, the XANES or ELNES spectra of many complex crystals have been calculated using the supercell-OLCAO method.[28–30,44,45] In the present work, we have calculated the K edges (Al, Si, and C) and L_3 edges (Al, and Si) of atoms at all crystallographically nonequivalent sites in the Al_4SiC_4 crystal. As emphasized in many recent publications,[29,44,45] the total spectrum for a particular edge of a given element should be the weighted sum of the spectra from individual sites, which will be slightly different

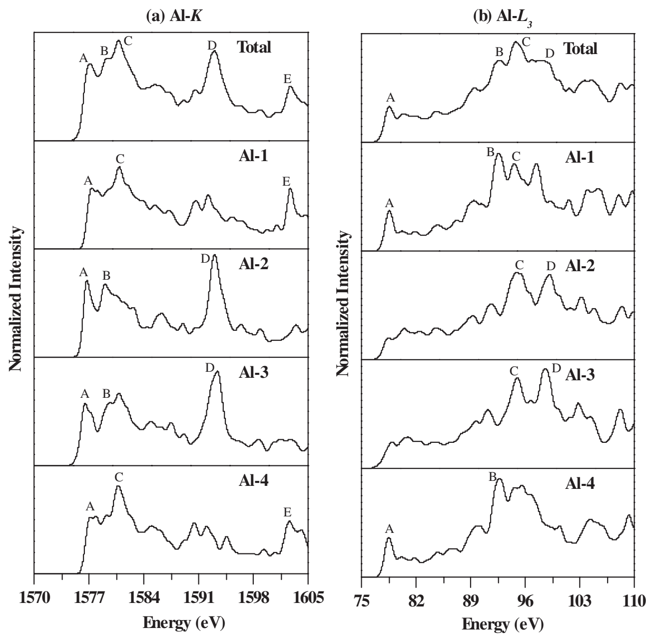

FIG. 8. Calculated K and L edges for Al in Al_4SiC_4.

from each other depending on their different local bonding environments. The weighting factor is proportional to the number of site occupation of that element.

The calculated XANES or ELNES spectra (Al-K, Al-L_3, Si-K, Si-L_3, and C-K edges) of Al_4SiC_4 are shown in Figs. 8–10. Since $Al_4Si_2C_5$ has a similar crystal structure and local bonding environment as Al_4SiC_4, we limited our calculations to Al_4SiC_4 only. A $3\times3\times1$ supercell of 162 atoms was used in the calculation which is sufficiently large to avoid any interactions between the core holes. The total spectrum for each atom is shown at the top panel with those at different sites shown in the lower panels. The spectra of Al-K from different sites are different due to the different bonding environments of Al atoms discussed earlier. The main peaks in the total Al-K [Fig. 8(a), top panel] are marked as A, B, C, D, and E. Peak D (1593 eV) is the most prominent and its main contributors are from the Al-2 and Al-3. Peak C at 1580 eV

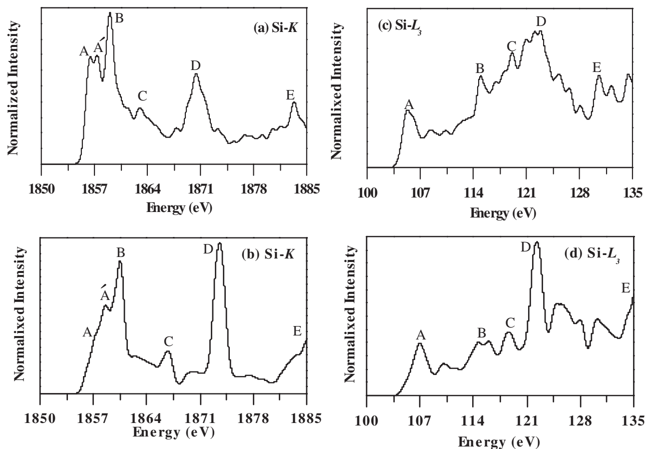

FIG. 9. Calculated [(a) and (b)] Si-K edges and [(c) and (d)] Si-L_3 edges in [(a) and (c)] Al_4SiC_4 crystal and in [(b) and (d)] 3C-SiC.

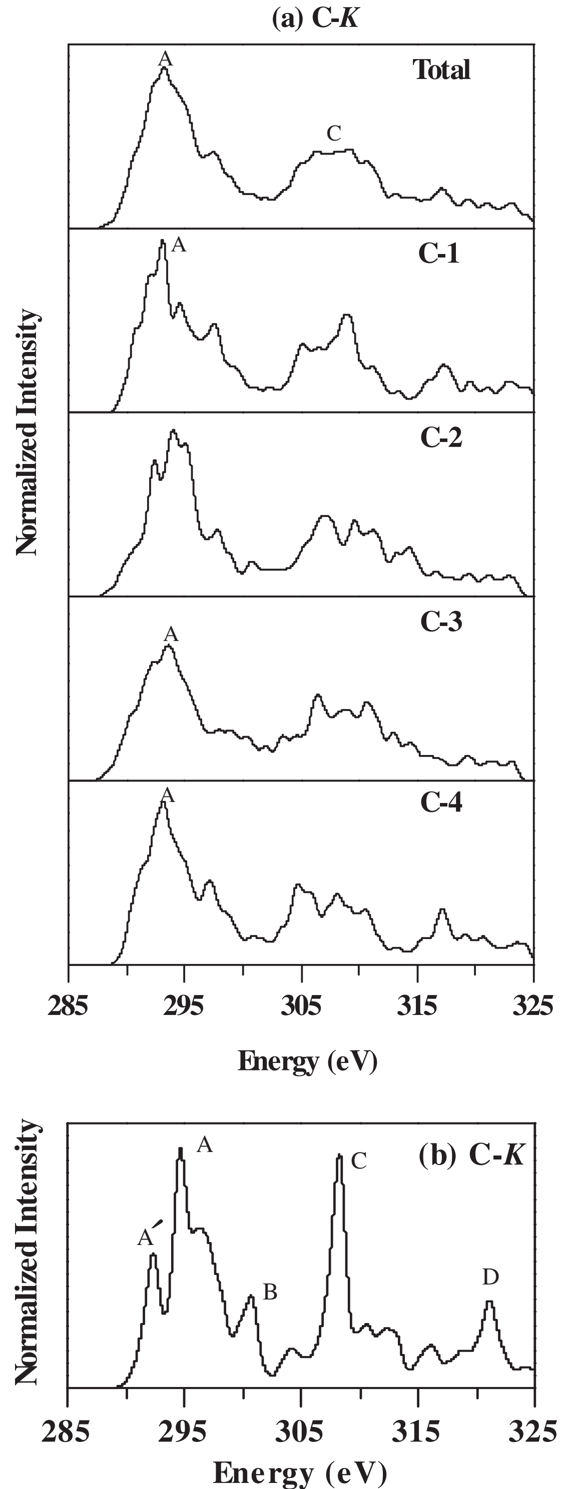

FIG. 10. Calculated C-K edges in (a) Al_4SiC_4 crystal, and in (b) 3C-SiC.

comes mostly from Al-1 and Al-4. The peak at the leading edge of the onset is labeled as A (1577 eV) and is contributed by all Al ions (less from Al-1 and Al-4). On the other hand, peak E (1602 eV) in the total spectrum is mostly from the Al-1 and Al-4. Peak B in the total spectrum appears as a short shoulder at 1579 eV which arises from Al-2 B. For the Al-L_3 edge, the total spectrum shown at the top panel of Fig.

8(b) has two strong peaks *A* (79 eV) and *C* (95 eV), and two weaker peaks *B* (93 eV) and *D* (99 eV). A results from Al-1 and Al-4. *C* results from Al-2 and Al-3. On the other hand, peak *B* arises from Al-1 and Al-4, and *D* is from the Al-2 and Al-3. These results indicate that (Al-1, Al-4) pair and (Al-2, Al-3) pair make unique contributions to the total absorption spectrum at different energy ranges.

In the Si-*K* edge shown in Fig. 9(a), there are three strong peaks *B* (1857 eV), *D* (1870.41 eV), and *E* (1883 eV), a weaker peak *C*, and a double peak *A* and *A′* at the edge onset (1856 and 1857 eV). These five prominent structures in Si-*K* edge bear some resemblance to the Al-*K* edge spectrum discussed above since they both probe the *p* states ($\ell = 1$) in the conduction band of Al_4SiC_4. The Si-*K* edge spectrum presented here is compared to that of 3C-SiC (Ref. 34) shown in Fig. 9(b). We observe that the five prominent spectral features are also present in SiC but with different intensities, especially in peak *D*. In 3C-SiC, the leading edge in the Si-*K* edge has a much larger slope resulting in large difference with the *A*, *A′* double peak in Al_4SiC_4. These differences are obviously due to the difference in the local environment of the two crystals. For the Si-L_3 spectrum [Fig. 9(c)], we again have observed five peaks (*A*, *B*, *C*, *D*, and *E*) at 105, 115, 119, 123, and 131 eV, respectively. The Si-L_3 is very different from the Si-*K* edge since it probes the unoccupied ($s + d$) states ($\ell = 0$ or 2) in the CB. In the first 10 eV range, there is only one prominent peak *A* at the leading edge. There are then many structures in the higher energy range which can be roughly assigned as four peaks. Again, the Si-L_3 spectrum presented here is quite different from the one presented in Fig. 9(d) for SiC especially in peak *A* and the main peak *D*.

The total C-*K* spectrum [Fig. 10(a)] has one prominent peak *A* (293 eV) and a much broadened structure C (307 eV) contributed by all four carbon sites C-1, C-2, C-3 and C-4. The overall features of the spectra at four C sites are not too different from the combined one. Compared with the same C-*K* edge from 3C-SiC [Fig. 10(b)], we observe that the later is sharper and better resolved compared to the more broadened spectra from Al_4SiC_4 although peaks *A* and *C* are still the dominating features. This is again due to the difference in the local atomic arrangements surrounding C in these two crystals.

V. CONCLUSIONS

We have presented a detailed calculation of the electronic structure and spectral properties of two ternary carbides Al_4SiC_4 and $Al_4Si_2C_5$ using the *ab initio* OLCAO method. Both are semiconductors with indirect band gaps of 1.05 and 1.02 eV, respectively. The electron effective mass of Al_4SiC_4 is comparable to other semiconductors such as Ge and Si while the hole effective masses in both crystals are very large. However, it is noted that the parallel component of the electron effective mass in $Al_4Si_2C_5$ is almost 5.5 times as large as that in $Al_4Si_2C_5$ which we tentatively attribute to the exceptionally long *c* axis in the later crystal. Mulliken effective charge calculations shows considerable charge transfer from Al and Si to C. However, the amount of charge transfer is similar in both crystals Al_4SiC_4 and $Al_4Si_2C_5$. The estimated refractive index of the calculated dielectric function shows a slightly larger value for Al_4SiC_4 than $Al_4Si_2C_5$. Both crystals exhibit strong birefringence in the optical spectra. The calculated XANES or ELNES spectra for Al_4SiC_4 show rich structures and are more broadened than those in simpler crystals such as cubic SiC. These calculated XANES or ELNES spectra are considered to be theoretical predictions and can be used to compare with experimental measurements yet to be carried out. The results presented in this paper show that hexagonal ternary Al-Si-C ceramic compounds have some very unique electronic and optical properties. When combined with their outstanding structural and mechanical properties mentioned in Sec. I, the range of applications of these remarkable materials in different industrial sectors can be significantly expanded. It is highly desirable that additional experimental work be carried out to verify the predicted properties presented in this paper.

ACKNOWLEDGMENTS

Altaf Hussain is thankful to the Department of Physics, University of Missouri-Kansas City (UMKC) for providing local hospitality. He is also thankful to the Higher Education Commission (HEC) of Pakistan for supporting financially and making it possible for him to work at UMKC (USA). W.Y.C. was supported by U.S. Department of Energy under Grant No. DE-FG02-84PR45170.

*Corresponding author; altaf4ever@hotmail.com

[1] J. F. Huang, X. R. Zeng, H. J. Li, X. B. Xiong, and M. Huang, Mater. Lett. **58**, 2627 (2004).
[2] M. W. Barsoum, Prog. Solid State Chem. **28**, 201 (2000).
[3] J. C. Schuster and H. Nowotny, Z. Metallkd. **71**, 341 (1980).
[4] J. Y. Wang, Y. C. Zhou, Z. J. Lin, T. Liao, and L. F. He, Phys. Rev. B **73**, 134107 (2006).
[5] J. V. Foltz and C. M. Blackmon, in *Metal Matrix Composites, ASM Handbook*, 10th ed. ASM-international (Metals Park, OH, 1998), Vol. 2.
[6] P. Rodriguez and J. M. Fusaro, in *Proc. Adv. Electron. Packag. 1997—Pacific Rim/ASME Int. Electron. Packag. Conf.—InterPak'97*, Vol. EEP-19-2, p. 2173–2178.
[7] A. R. Kennedy, D. P. Weston, M. I. Jones, and C. Enel, Scr. Mater. **42**, 1187 (2000).
[8] H. Yokokawa, M. Fujita, S. Ujiie, and M. Dokiya, Metall. Trans. B **18**, 433 (1987).
[9] X. X. Huang, G. W. Wen, X. M. Cheng, and B. Y. Zhang, Corros. Sci. **49**, 2059 (2007).
[10] K. Inoue, S. Mori, and A. Yamaguchi, J. Ceram. Soc. Jpn. **111**, 348 (2003).
[11] K. Inoue, A. Yamaguchi, and S. Hashimoto, J. Ceram. Soc. Jpn.

110, 1010 (2002).
[12] K. Inoue and A. Yamaguchi, J. Ceram. Soc. Jpn. **111**, 267 (2003).
[13] X. X. Huang and G. W. Wen, Ceram. Int. **33**, 453 (2007).
[14] G. W. Wen and X. X. Huang, J. Eur. Ceram. Soc. **26**, 1281 (2006).
[15] V. L. Solozhenko and O. O. Kurakevych, Solid State Commun. **135**, 87 (2005).
[16] T. Liao, J. Wang, and Y. Zhou, Phys. Rev. B **74**, 174112 (2006).
[17] Z. Inoue, Y. Inomata, H. Tanaka, and H. Kawabata, J. Mater. Sci. **15**, 255 (1980).
[18] W. Y. Ching, J. Am. Ceram. Soc. **73**, 3135 (1990).
[19] Z. Inoue, Y. Inomata, H. Tanaka, and H. Kawabata, J. Mater. Sci. **15**, 575 (1980).
[20] G. A. Jeffrey and V. Y. Wu, Acta Crystallogr. **20**, 538 (1966).
[21] G. Kresse and J. Furthmuller, Comput. Mater. Sci. **6**, 15 (1996); Phys. Rev. B **54**, 11169 (1996).
[22] N. Soga, J. Geophys. Res. **72**, 4227 (1967).
[23] D. Vanderbilt, Phys. Rev. B **41**, 7892 (1990).
[24] J. P. Perdew, J. A. Chevary, S. H. Vosko, K. A. Jackson, M. R. Pederson, D. J. Singh, and C. Fiolhais, Phys. Rev. B **46**, 6671 (1992).
[25] H. J. Monkhorst and J. D. Pack, Phys. Rev. B **13**, 5188 (1976).
[26] W. Y. Ching, J. Am. Ceram. Soc. **87**, 1996 (2004).
[27] P. Rulis, Hongzhi Yao, L. Ouyang, and W. Y. Ching, Phys. Rev. B **76**, 245410 (2007).
[28] W. Y. Ching and P. Rulis, Phys. Rev. B **77**, 035125 (2008).
[29] W. Y. Ching and P. Rulis, Phys. Rev. B **77**, 125116 (2008).
[30] R. S. Mulliken, J. Am. Chem. Soc. **23**, 1833 (1955); **23**, 1841 (1955).
[31] J. P. Perdew and A. Zunger, Phys. Rev. B **23**, 5048 (1981).
[32] S. M. Sze and Kwok K. Ng, *Physics of Semiconductor Devices*, 3rd ed. (Wiley, New York, 2006).
[33] Walter A. Harrison, *Electronic Structure and the Properties of Solids* (Freeman, San Francisco, 1980).
[34] W. Y. Ching, Y. N. Xu, P. Rulis, and L. Ouyang, Mater. Sci. Eng., A **422**, 147 (2006).
[35] M. Born and E. Wolf, *Principles of Optics*, 7th ed. (Cambridge University Press, Cambridge, 1999).
[36] V. J. Barczak, J. Am. Ceram. Soc. **44**, 299 (1961).
[37] See, for example, D. A. Muller, T. Sorsch, S. Moccio, F. H. Baumann, K. Evans-Lutterodt, and G. Timp, Nature (London) **399**, 758 (1999).
[38] S.-D. Mo and W. Y. Ching, Phys. Rev. B **62**, 7901 (2000).
[39] W. Y. Ching, S. D. Mo, and Y. Chen, J. Am. Ceram. Soc. **85**, 11 (2002).
[40] W. Y. Ching and P. Rulis, Phys. Rev. B **73**, 045202 (2006).
[41] T. Mizoguchi, I. Tanaka, S. Yoshioka, M. Kunisu, T. Yamamoto, and W. Y. Ching, Phys. Rev. B **70**, 045103 (2004).
[42] I. Tanaka, T. Mizoguchi, M. Matsui, S. Yoshioka, H. Adachi, H. Yamamoto, T. Okajima, M. Umesaki, W. Y. Ching, Y. Inoue, M. Mizuno, H. Araki, and Y. Shirai, Nature Mater. **2**, 541 (2003).
[43] P. Rulis, W. Y. Ching, and M. Kohyama, Acta Mater. **52**, 3009 (2004).
[44] S. Aryal, P. Rulis, and W. Y. Ching, Am. Mineral. **93**, 114 (2008).
[45] W. Y. Ching, L. Ouyang, Paul Rulis, and Hongzhi Yao, Phys. Rev. B **78**, 014106 (2008).